In-situ observation of the behaviour of non-metallic inclusions at different interfaces in the system steel-slag-refractory

S K Michelic[1], U Diéguez Salgado[1] and C Bernhard[1]

[1] Chair of Ferrous Metallurgy, Montanuniversitaet Leoben, Franz Josef Straße 18, 8700 Leoben, Austria
E-Mail: susanne.michelic@unileoben.ac.at

Abstract. The system steel-slag-refractory and reactions of non-metallic inclusions at its interfaces are decisive in numerous metallurgical processes. In order to obtain the desired steel cleanness level, a detailed understanding of the occurring interactions is needed. This study focuses on the in-situ observation of reactions of inclusions at different interfaces between steel, slag and refractory material. For this purpose a Confocal Scanning Laser Microscope attached to a high temperature furnace is applied which enables the visualization of metallurgical phenomena at steelmaking temperatures up to 1700 °C. Two different examples are discussed: First, the agglomeration of different inclusion types in a Ca-treated steel is described and corresponding attraction forces are calculated. Secondly, the dissolution of Al_2O_3 and $MgOAl_2O_3$ in two slags of the system $CaO\text{-}Al_2O_3\text{-}MgO\text{-}SiO_2$ is examined, including the evaluation of the governing dissolution mechanism. Finally, an outlook on further experimental possibilities is given.

1. Introduction

Number, size and composition of non-metallic inclusions in the steel matrix directly influence the final product quality for a broad field of steel grades. Thus, a specific adjustment of steel cleanness in secondary metallurgical processes is essential in order to avoid problems in the subsequent casting process, e.g. clogging as well as to achieve the required quality level. Principally, the phases steel, slag and refractory material determine and influence the behavior of non-metallic inclusions. Different reaction sites involving these phases exist. Next to the agglomeration of inclusions in the liquid steel, their separation from the steel to the slag, and their subsequent dissolution in the slag has to be considered. Additionally, inclusions can be modified through the contact with refractory material or slag.

High-temperature Confocal Scanning Laser Microscopy (HT-CSLM) offers a relatively new approach for in-situ investigations of reactions at temperatures relevant to steelmaking processes. Based on the pioneer work done by Japanese researchers [1], this method is applied for the investigation of phase transformations [2, 3] as well as inclusion related questions [4–6]. Within the present study the application of CSLM is shown for two different cases. As a first example, the agglomeration of different inclusion types in a Ca-treated steel is illustrated and the calculation of the corresponding attraction forces between a particle pair is described. Secondly, the dissolution behavior of Al_2O_3 and $MgOAl_2O_3$ in two slags of the system $CaO\text{-}Al_2O_3\text{-}MgO\text{-}SiO_2$ is investigated. Absolute dissolution times as well as the dissolution mechanism are evaluated.

2. The Method

2.1. Experimental Set-Up

A Confocal Scanning Laser Microscope type VL2000DX from Lasertec and a high temperature furnace type SVF17-SP from Yonekura are used for all investigations. The decisive advantage of HT-CSLM in contrast to conventional microscopes or experimental facilities is the possibility of in-situ observations at temperatures up to 1700 °C in combination with a very good image quality. This is primarily possible due to the fact, that a laser is used as a light source. The laser is characterized by a wavelength of 408 nm and is therewith below the thermal radiation spectrum of the observed samples. So, the contrast of the image can be increased significantly. Heat is provided by a halogen lamp with a maximum power of 1500 W. In combination with a low sample weight, this enables heating rates up to 1200 °C and cooling rates of 1000 °C/min. The maximum operating temperature is about 1700 °C at standard configurations and is only limited by the thermocouple type. Since the high temperature furnace is cooled, the thermal strain for the furnace through the radiation source is comparably low. Through the use of an acousto-optic element a very high scan rate can be reached. For the maximum resolution of 1024x1024, 15 images per second are stored. A resolution of 1024x256 enables the recording of 60 images per second [7]. A schematic view of the experimental set-up in the high temperature furnace which shows an elliptic, gold coated inner contour can be found in [7]. The halogen lamp is situated in the bottom focal point. The sample holder with the crucible and sample inside is located in the top focal point of the ellipse. The temperature is measured with a thermocouple fixed at the bottom side of the sample holder. The position of the thermocouple always results in a temperature difference between the sample surface and the thermocouple. Therefore an accurate temperature calibration is necessary before the experiment itself. High-purity argon with a flow rate of 100 cm^3/min ensures a neutral atmosphere in the furnace. Additionally, the oxygen content in the furnace is measured for every experiment. The latter typically lies in the range of 10-18 ppm during the experiment.

2.2. Experimental Procedure

Various experiments can be performed with the described set-up. In the present study two different experimental procedures are applied studying the cases of inclusion agglomeration in the liquid steel and inclusion dissolution in a slag phase. Figure 1 gives an overview on the used experimental set-ups for these two types of investigations:

- For type 1 experiments a steel disc with 600µm thickness is placed in an Al_2O_3 crucible and subsequently set up on the sample holder of the ellipsoidal furnace. The specimen is heated up following the heating cycle given in Figure 2. An alumina disc is placed under the steel disc in order to avoid the attachment of the steel disc onto the crucible.When the liquidus temperature of the steel is reached, inclusions are starting to emerge from the bulk to the steel surface and their agglomeration behavior can be studied. A posteriori examination of the sample at room temperature is carried out using a Scanning Electron Microscope with Energy Dispersive X-Rays (SEM/EDS). In order to characterize (composition, shape, size) the inclusions observed during the experiment, a fast cooling of the sample is important. In the present study a Ca-treated steel is used (composition given in Table 1).

- For type 2 experiments involving a slag phase a platinum crucible is used instead of Al_2O_3. A well-shaped spherical inclusion particle with a known diameter is placed on the surface of the defined amount of premolten slag in the crucible (compositions given in Table 1). Figure 2 shows a typical heating cycle for dissolution experiments. The whole assembly is heated up to the target temperature using the maximum heating rate. This is important to ensure that the inclusion hardly starts to dissolve before the experimental temperature is reached. At a

temperature 50 °C below the final temperature, the heating rate is reduced to 100°C/min in order to avoid overshooting. The experimental temperature can be defined arbitrarily up to 1700 °C. In the present study inclusion dissolution is examined at 1450 °C.

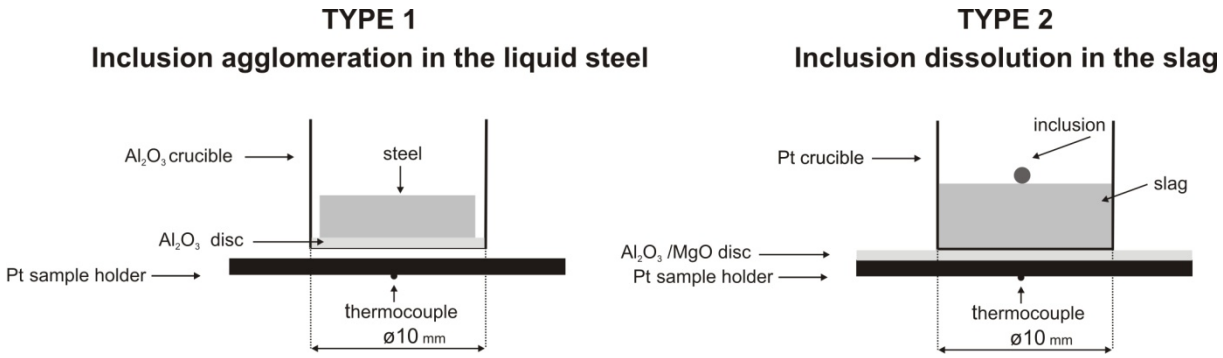

Figure 1. Experimental set-ups for the two experiments.

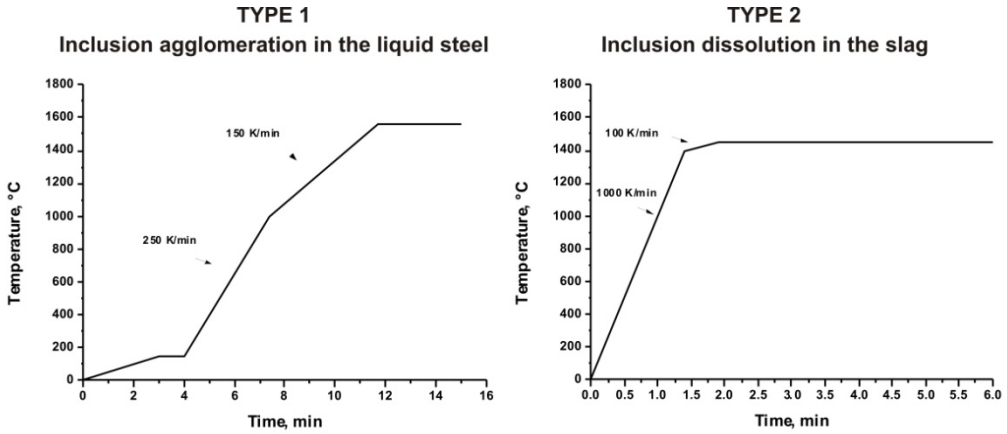

Figure 2. Time-temperature profiles of the two experimental types.

Table 1: Investigated materials.

Steel	**C [wt.-%]**	**Si [wt.-%]**	**Mn [wt.-%]**	**Al [wt.-%]**	**Ca [wt.-%]**	**S [wt.-%]**
	0.15	0.02	1.07	0.04	0.0012	0.004
Slags	**CaO [wt.-%]**	**Al_2O_3 [wt.-%]**	**MgO [wt.-%]**	**SiO_2 [wt.-%]**		
Slag 1	40	52	5	3		
Slag 2	33	3	12	52		
Inclusion	Al_2O_3 $MgOAl_2O_3$					

3. In-situ Observations

3.1. Inclusion Agglomeration in Liquid Steel

Inclusion formation during steel processing is unavoidable. The harmful effects of inclusions can be reduced if inclusion chemistries and morphologies are tailored properly and they can even be rendered beneficial in specific cases. In order to optimize steel cleanness in different process steps, a detailed understanding of the factors influencing agglomeration and coalescence of inclusions in molten steel is necessary. In addition to fluid dynamics, interfacial chemical interactions between particles are

important [8–10]. Several research groups already dealt with this topic in the last years especially focusing on the in-situ observation of the agglomeration process and the resultant quantitative evaluation of the obtained data. For example, Yin et al. [6, 11] described the behavior of alumina inclusions at a steel-gas interface. They found out that the non-wettability behavior of the alumina based non-metallic inclusions generate a deformation of the liquid surface, which is called meniscus. If two particles approach one-another, the meniscus in between them is further depressed or drawn downward [12]. This change, which is called capillary attraction, can lead to a difference of capillary pressure between the inside and the outside area of the pair, which will push the two bodies towards each other [11]. The capillary attraction is believed to be the source of the attraction between alumina inclusions at free surfaces and at gas bubbles inside the liquid steel melt [12]. The strength of the capillary attraction force for inclusion particle pairs in molten steel, which was found to be much different for particles with different morphology, can be listed as follows in ascending order [6]: liquid/liquid pair < liquid/semiliquid pair < semiliquid/semi-liquid pair < liquid/solid pair < semiliquid/solid pair and finally solid/solid pair as the strongest. The latter sequence is only valid if only the effect of the particle morphology is considered. But the attraction between particles is also strongly affected by other parameters like for example by the particle size, the contact angle of a particle with steel melt, the particle density, the shape and the interfacial tension [13].
Yin et al. [11] carried out an approximate evaluation of the magnitude of the attraction force from measured acceleration and estimated the mass of particles based on in-situ observations in the confocal microscope. The particle shape was approximated to be an ellipse disk and the lengths of long axis (d_1) and short axis (d_2) of a particle were observed. The height of all the disks was taken to be 2µm on the basis of confocal observations of the thickness of alumina particles on steel melt surface. Further, the ellipse was approximated to be a round disk of the radius, r, which was taken to be geometric average according to Equation 1.

$$r = \sqrt{d_1 \cdot d_2/2} \tag{1}$$

The acceleration, a_1, of the guest particle when the host particle in the particle pair stayed quiescent was determined from the change of the position of the guest particle at defined intervals. The force F was subsequently calculated by

$$F = m_1 a_1 \tag{2}$$

where m_1 is the mass of the guest particle (the moving particle toward a bigger one). If the size difference between two particles in a particle pair was big, then the smaller one in the pair (the guest particle) moved accelerated toward the larger one (the host particle), which was almost quiescent while attraction took place. On the contrary, if the pair of particles were almost the same size, then both particles moved accelerative to make a head-on collision. If both inclusions move, a correction factor for the mass m_1 was used:

$$\frac{m_2}{m_1+m_2} \tag{3}$$

where m_2 is the mass of the largest inclusion. In this force analysis, the friction force that arises from the viscous drag of the particle by liquid steel surface was ignored.

This approach was applied for the investigations in the present study, evaluating the agglomeration behavior of liquid and semiliquid non-metallic inclusions in a Ca-treated steel (composition given in Table 1). Figure 3 exemplarily shows results of inclusion agglomeration experiments (type 1) in a Ca-treated steel. After a large part of the sample surface melted, many inclusion particles emerged from the interior of molten steel bath and floated on the melt surface. After the experiment itself the sample was cooled down as fast as possible in order to analyze the inclusion composition using a Scanning Electron Microscope with Energy Dispersive X-Rays (SEM/EDS). Figure 4a shows a SEM- image of a specimen at room temperature after conducting the HT-CSLM experiment. Almost all the surfaced

inclusion particles from the calcium treated steel melt were observed to be in semi-liquid irregular shape and liquid with globular shape. Representative examples of detected inclusions are given in Figure 4b and c. Their chemical composition is summarized in Table 2. The semi-liquid inclusions are composed by two different phases; the calcium sulfide with traces of calcium oxide phase is solid and the calcium aluminate phase is liquid (Figure 4b). The liquid inclusions are composed of calcium aluminate (Figure 4c).

When no local surface flow was observed, the semiliquid and liquid inclusions showed no attraction between them (Figure 3a). When one liquid particle floats up to the melt surface, it pushes neighboring particles until separation is sufficient (Figure 3b and Figure 3c); finally, the original state of dispersion is reached (Figure 3d), they exhibit no relative movement during the experiment, indicating no change of distance between particles, and moving with random direction.

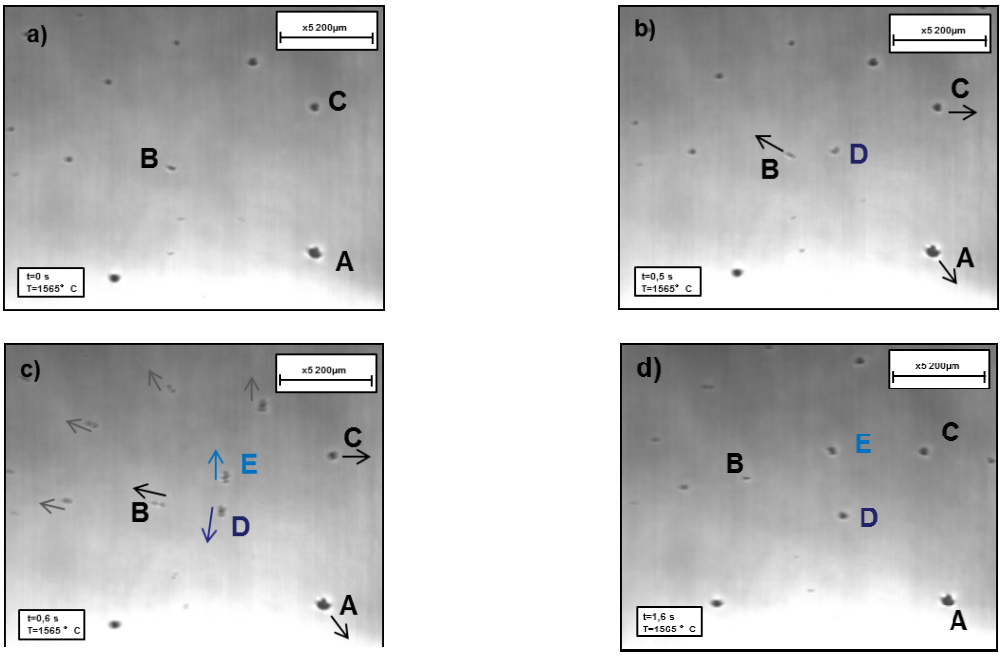

Figure 3. (a) Semiliquid particles distributed on the melt surface homogeneously (b) one particle D floats up and pushes the neighboring particles A, B and C (c) a new particle E floats up and again the neighboring particles move (d) the particles are distributed on the melt surface.

Since the contact angle of non-metallic inclusions and steel melt is usually more than 90°, the capillary force will become weak with decreasing density of inclusion particle and contact angle. The contact angle between semiliquid particles and melt is smaller since the liquid layer results in good wetting; this means that the capillary force between semiliquid particles in pairs will be weaker than for solid particles in pairs in agreement with [6,15]. Nevertheless, some interaction between the inclusions is observed close to the solidification front. In Figure 5a some semiliquid as well as liquid inclusions are observed in the pool close to the solidification front; these inclusions seem to be quiet. A single semiliquid inclusion (approx.12µm diameter) appears in the middle of the pool and after 2 second collides with another semiliquid inclusion (approx. 30µm). The trajectory of the particle is observed in Figure 5 as a function of the time. The velocity of the small particle increases when the distance between both particles is decreasing, showing that there is an increasing attraction force between this particle pair which helps them to finally agglomerate.

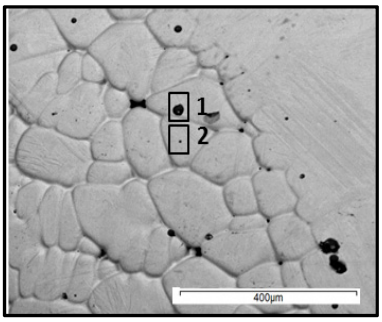

Figure 4a. SEM- image of a specimen at room temperature after HT-CSLM experiment.

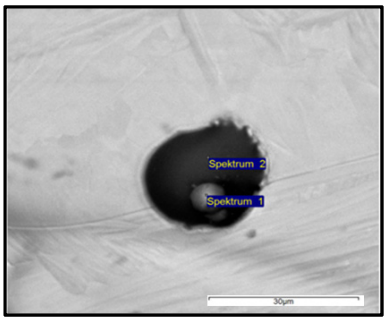

Figure 4b. Square 1 from Figure 6a.Semi-liquid inclusion with 22µm diameter, its composition given in Table 2.

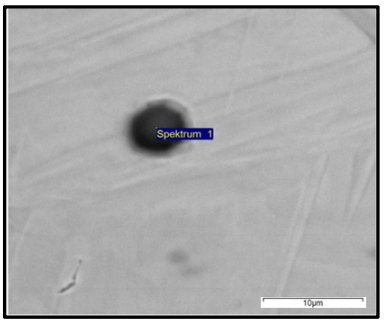

Figure 4c. Square 2 from Figure 6a. Liquid globular inclusion with 5µm diameter, its composition given in Table 2.

Table 2: SEM/EDS analyses for inclusions illustrated in Figure 4b and c.

Fig.	Spec.	O [wt.-%]	Al [wt.-%]	S [wt.-%]	Ca [wt.-%]	Mn [wt.-%]	Fe [wt.-%]	Phase
4b	1	11.9	0.5	39.7	45.1	0.7	2.1	Oxisulfide
	2	46.9	28.8	0.3	20.3	2.7	1.0	Al-Ca-Oxide
4c	1	43.8	30.6	1.4	16.7	1.2	6.3	Al-Ca-Oxide

Figure 6 displays the results of the measured interparticle distances as a function of time and the hence calculated attraction force for the pair of semiliquid inclusions shown in Figure 5. Principally, the tendency of agglomeration for liquid as well as for semiliquid inclusions is smaller than for solid inclusions. According to literature [6] the attraction force of a pair of semiliquid CA60 particles is approximately 10^{-16} -10^{-15} N, which agrees well with the results shown in Figure 6.

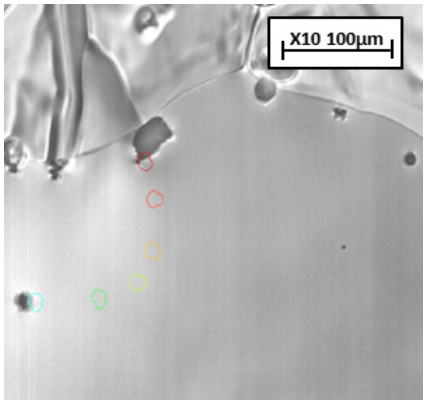

Figure 5. Attachment of inclusions at the solidification front in the Ca-treated steel.

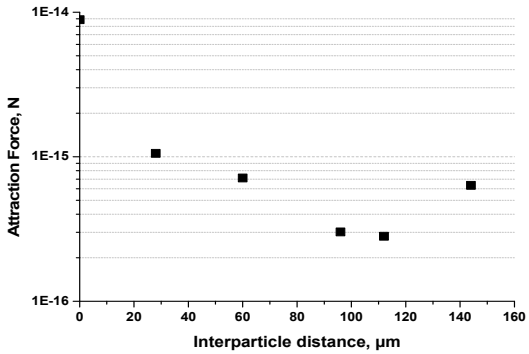

Figure 6. Attraction force versus interparticle distance for the semiliquid inclusion pair shown in Figure 5.

3.2. Inclusion Dissolution in the Slag Phase

In the last years the confocal laser scanning microscope frequently replaced classical post-mortem studies [15, 16], dipping or rotating a shaped oxide material into a liquid slag, for investigating the

dissolution behavior of various oxides in different slag compositions. The main focus of previous in-situ studies with the CLSM lied on the dissolution of Al_2O_3, MgO and $MgAl_2O_4$ in CaO-Al_2O_3-SiO_2 or CaO-Al_2O_3-SiO_2-MgO slags [17–23]. A first output of the dissolution experiments is the absolute dissolution time which is based on the evaluation of decreasing particle diameter with ongoing time. Details regarding the evaluation procedure based on the obtained video from CSLM can be found in [24]. Next to the comparison of absolute dissolution rates of different particles in defined slag composition also the governing dissolution mechanism got in the focus of interest. For this purpose normalized dissolution graphs (transient diameter divided by initial diameter and time divided by total dissolution time) are used. In order to determine the dissolution mechanism different models are proposed in literature: The analytical solution using the Shrinking Core Model (SCM) has been widely applied. [17, 21, 22, 25] In this model either the chemical reaction at the interface between inclusion and slag (linear correlation between particle size and dissolution time) or the mass transport of the dissolving particle in the boundary layer of the slag (parabolic dependence) can be the rate controlling step for the dissolution. Further details of this model are given in literature [26].

Another approach was proposed by Verhaeghe et al. [27–29] using a diffusion equation coupled with Lattice-Boltzmann modeling. Due to the high computational effort needed, it is less applied although its results are usually more accurate. Approximations of the diffusion equation for spherical particles are suited to analyze if the dissolution is governed by diffusion or not. Dissolution controlled by diffusion in a stagnant fluid can generally be described by Fick's first and second law of diffusion. [30] Principally, it has to be distinguished between invariant interface (resulting in an S-shaped normalized dissolution curve) and invariant field approximation (parabolic normalized dissolution curve). Details regarding the two approximations as well as the complete derivation can be found in [24].

A modified diffusion model based on the use of well-shaped spherical particles was introduced by Feichtinger et al. [24] merging the two approaches described above and introducing an additional factor f :

$$\frac{dR}{dt} = -\frac{k \cdot D}{R} - f \cdot k \cdot \sqrt{\frac{D}{\pi \cdot t}} \tag{4}$$

This approach focuses on the influence of slag viscosity on the governing dissolution mechanism. As equally assumed for all other mentioned models, the formation of a solid layer around the inclusion during dissolution cannot be considered with this approach.

In the present study the dissolution behavior of Al_2O_3 and $MgOAl_2O_3$ is examined in two different slag compositions in the system CaO-Al_2O_3-SiO_2-MgO at a temperature of 1450 °C: Slag 1 characterized by a high Al_2O_3 content and slag 2 contains SiO_2 as the main component. All thermodynamic data (e.g. saturation concentration of Al_2O_3 and $MgOAl_2O_3$ in the particular slag) as well as slag viscosities needed for the evaluation were calculated by *FactSage 6.4*. Slag densities were taken from literature [31]. Slag 2 is characterized by a significant higher viscosity (0.58 Pas) than slag 1 (0.23 Pas). Detailed slag compositions are summarized in Table 1. As already described the viscosity can essentially influence the governing dissolution mechanism and therewith the shape of the normalized dissolution curve between S-shape and parabolic shape.

A comparison of absolute dissolution times for Al_2O_3 and $MgOAl_2O_3$ in the two investigated slags is given in Figure 7. For each case three experiments were carried out; for the evaluation of the dissolution mechanism the mean out of the three experiments was used. Both inclusion types dissolved significantly faster in slag 1 compared to slag 2. Furthermore, the dissolution of Al_2O_3 was always observed to be faster than the $MgOAl_2O_3$ dissolution process. A comparison with data available in

literature is difficult due to the at least small deviations in examined slag compositions as well as in experimental temperature, which already can influence the results noticeably.

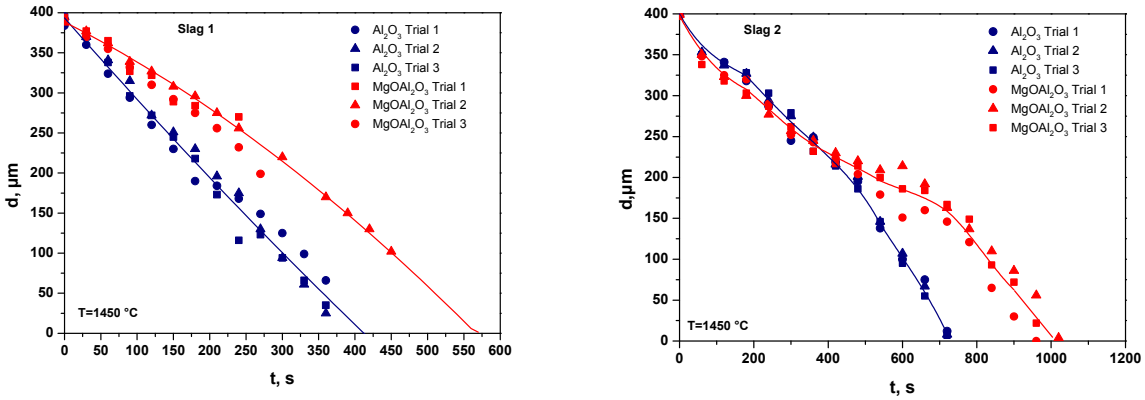

Figure 7: Comparison of absolute dissolution rates of Al_2O_3 and $MgOAl_2O_3$ in slags 1 and 2.

Figure 8 summarizes the results concerning the evaluation of the governing dissolution mechanism. Figures 8a and 8b compare the normalized dissolution curves to classical models from literature. It can be seen that only one case – the dissolution of Al_2O_3 in slag 1 – can be described sufficiently. The latter case shows an almost linear dependence and therefore can be reflected by the reaction rate controlled Shrinking Core Model. The other three cases do not match with the classical approaches. Here, the previously discussed modified diffusion model introduced by Feichtinger et al. [24] was applied. The obtained results are given in Figure 8c, including the used f-factor. The same dependence as already observed in former studies [24] is found: Increasing slag viscosity changes the dissolution pattern from parabolic (characterized by a low f-factor) to S-shaped (characterized by a high f-factor).

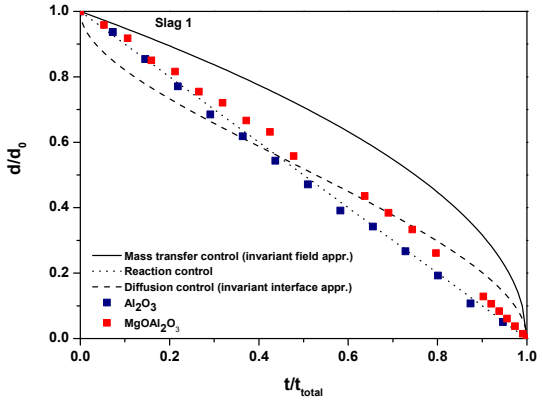

Figure 8a. Normalized dissolution curves for Al_2O_3 and $MgOAl_2O_3$ in slag 1 including classical dissolution models from literature.

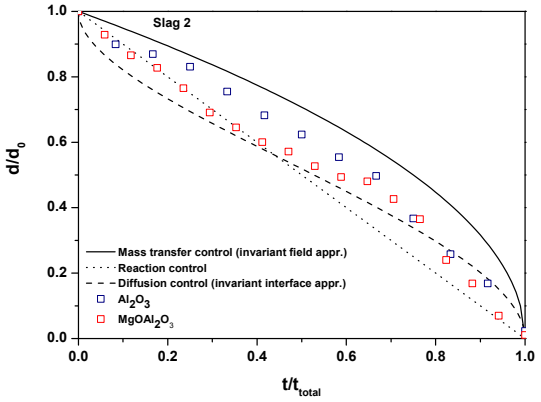

Figure 8b. Normalized dissolution curves for Al_2O_3 and $MgOAl_2O_3$ in slag 2 including classical dissolution models from literature.

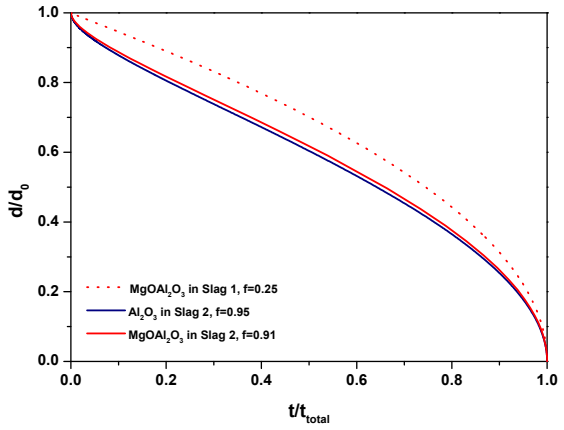

Figure 8c: Normalized dissolution patterns for $MgOAl_2O_3$ in slag 1 and Al_2O_3 and $MgOAl_2O_3$ in slag 2 calculated using the modified diffusion model introduced by Feichtinger et al.

4. Summary and Conclusion

Different reactions and interactions of non-metallic inclusions within in the system steel-slag-refractory can essentially influence the final steel cleanness – in a positive or negative way. Within the present work two types of inclusion reactions are described applying Confocal Scanning Laser Microscopy:

- Inclusion agglomeration in a Ca-treated low carbon steel: The tendency of agglomeration for liquid as well as for semiliquid inclusions is smaller than for solid inclusions. The attraction force of a pair of semiliquid particles was determined with approximately 10^{-16} -10^{-15} N, which agrees well with literature.
- Dissolution of Al_2O_3 and $MgOAl_2O_3$ in the slag system $CaO\text{-}Al_2O_3\text{-}MgO\text{-}SiO_2$:$Al_2O_3$ proved to dissolve significantly faster than $MgOAl_2O_3$ in the investigated slags. Slag viscosity influences the dissolution mechanism essentially changing the pattern from parabolic to rather S-shaped with increasing slag viscosity.

Confocal Scanning Laser Microscopy does not only enable the in-situ observation of defined reactions on a microscopic scale but also provides important knowledge for processes on industrial scale, especially regarding the improvement of steel cleanness. Next to the two presented experimental types, also the reaction of inclusions at the interface steel-refractory can be studied. For example, these investigations can contribute to understand and evaluate the clogging sensitivity of certain steel-refractory combinations. Relating experiments are currently in progress.

Acknowledgements
Financial support by the Austrian Federal Government and the Styrian Provincial Government, represented by Österreichische Forschungsförderungsgesellschaft mbH and by Steirische Wirtschaftsförderungsgesellschaft mbH within the research activities of the K2 Competence Centre on "Integrated Research in Materials, Processing and Product Engineering", operated by the Materials Center Leoben Forschung GmbH in the framework of the Austrian COMET Competence Centre Programme, is gratefully acknowledged.

References

[1] Chikama H, Shibata H and Emi T 1996 *JIM Material Transactions* **37** 620–26
[2] Phelan D, Reid M, Stanford N and Dippenaar RJ 2006 *JOM* **58** 67–69
[3] Reid M, Phelan D and Dippenaar RJ 2004 *ISIJ Int.* **44** 565–72
[4] Misra P, Chevrier V, Sridhar S, Cramb AW 2000 *Metall. Mater. Trans. B* **31** 1135–39
[5] Shibata H, Yin H and Emi T 1998 *Phil Trans. R. Soc. Lond.* A **356** 957–66
[6] Yin H, Shibata H, Emi T and Suzuki M 1997 *ISIJ Int.* **37** 946–55
[7] Bernhard C, Schider S, Sormann A, Xia G and Ilie S 2011 *Berg- und Hüttenmännische Monatshefte* **156** 161–67
[8] Aneziris C G, Schroeder C, Emmel M, Schmidt G, Heller H P and Berek H 2013 *Metall. Mater. Trans. B* **44** 954–68
[9] Sasai K 2014 *ISIJ Int.* **54** 2780–89
[10] Coletti B, Vantilt S, Blanpain B and Sridhar S 2003 *Metall. Mater. Trans. B* **35** 533–38
[11] Yin H, Shibata H, Emi T and Suzuki M 1997 *ISIJ Int.* **37** 936–45
[12] Vantilt S, Coletti B, Blanpain B, Fransaer J, Wollants P and Sridhar S 2004 *ISIJ Int.* **44** 1–10
[13] Nakajima K and Mizoguchi S 2001 *Metall. Mater. Trans. B* **32** 629–41
[14] Luo H W 2001 *Scand. J. Metall.* 30 212–19
[15] Taira S, Nakashima K and Mori K 1993 *ISIJ Int.* **33** 116–23
[16] Yu X, Pomfret R J and Coley K S 1997 *Metall. Mater. Trans. B* **28** 275–79
[17] Liu J, Guo M, Jones P T, Verhaeghe F, Blanpain B and Wollants P 2007 *J. Eur. Ceram. Soc.* **27** 1961–72
[18] Monaghan B J and Chen L 2005 *Steel Research Int.* **76** 348–54
[19] Monaghan B J and Chen L 2006 *Ironmaking Steelmaking* **33** 323–30
[20] Monaghan B J, Chen L and Sorbe J 2005 *Ironmaking Steelmaking* **32** 258–64
[21] Sridhar S and Cramb AW 2000 *Metall. Mater. Trans. B* **31** 406–10
[22] Fox A B, Valdez M, Gisby J, Atwood R C, Lee P D and Sridhar S 2004 *ISIJ Int.* **44** 836–45
[23] Verhaeghe F, Blanpain B and Wollants P 2008 *Modell. Simul. Mater. Sci. Eng.* **16** 45007
[24] Feichtinger S, Michelic S K, Kang Y and Bernhard C 2014 *J. Am. Ceram. Soc.* **97** 316–25
[25] Monaghan B J and Chen L 2004 *J. Non-Cryst. Solids* **347** 254–61
[26] Levenspiel O 1999 *Chemical reaction engineering* vol 3 (New York: John Wiley & Sons)
[27] Verhaeghe F, Liu J, Guo M, Arnout S, Blanpain B and Wollants P 2008 *J. Appl. Phys.* **103** 23506
[28] Verhaeghe F, Liu J, Guo M, Arnout S, Blanpain B and Wollants P 2007 *Appl. Phys. Lett.* **91** 124104
[29] Verhaeghe F, Arnout S, Blanpain B and Wollants P 2005 *Phys. Rev. E* **72** 36308
[30] Whelan M J 1969 *Met. Sci.* **3** 95–97
[31] Slag Atlas, 2nd ed., Verlag Stahleisen GmbH, 1995.